Analytic gradient for the adaptive frozen orbital bond detachment in the fragment molecular orbital method

4 AUTHORS, INCLUDING:

Pavel Avramov
Siberian Federal University
92 PUBLICATIONS **522** CITATIONS

SEE PROFILE

Jan Halborg Jensen
University of Copenhagen
116 PUBLICATIONS **6,591** CITATIONS

SEE PROFILE

Analytic gradient for the adaptive frozen orbital bond detachment in the fragment molecular orbital method

Dmitri G. Fedorov [a,*], Pavel V. Avramov [b,c], Jan H. Jensen [d], Kazuo Kitaura [a,e]

[a] RICS, National Institute of Advanced Industrial Science and Technology (AIST), 1-1-1 Umezono, Tsukuba, Ibaraki 305-8568, Japan
[b] L.V. Kirensky Institute of Physics, SB RAS, Academgorodok, Krasnoyarsk 660036, Russia
[c] Siberian Federal University, 79 Svobodniy av., Krasnoyarsk 660041, Russia
[d] Department of Chemistry, University of Copenhagen, 2100 Copenhagen, Denmark
[e] Graduate School of Pharmaceutical Sciences, Kyoto University, Sakyo-ku, Kyoto 606-8501, Japan

ARTICLE INFO

ABSTRACT

We have developed and implemented the analytic energy gradient for the bond detachment scheme in the fragment molecular orbital method (FMO) suitable to describe solids, and applied it to the geometry optimization of a silicon nanowire at several levels of theory. In addition, we have examined in detail the effects of the particular choice of the fragmentation upon the accuracy and introduced a number of numerical criteria to characterize the errors. The established route is expected to provide guidance for future applications of FMO to surfaces, solids and nanosystems.

© 2009 Elsevier B.V. All rights reserved.

1. Introduction

Recent advances in quantum–mechanical methods have enabled their application to large systems of a nanoscale size, owing to the development of methodology and in considerable increase in the computational power. A large number of efficient methods has been developed, based on the full system Hamiltonian [1–3] and fragmentation approaches [4–13].

In the fragment molecular orbital method (FMO) [14–17] one performs quantum–mechanical calculations on fragments and their pairs in the electrostatic field of the remaining fragments, and many wave functions have been interfaced in the FMO framework [18–25]. The interaction energy analyses [26,27], geometry optimizations [28] and molecular dynamics [29] can be performed, and a number of applications demonstrate the usefulness of this method [30–32].

We have recently proposed the adaptive frozen orbital (AFO) bond detachment scheme in FMO [33] for the purpose of describing solids and surfaces. In the present Letter, we introduce the analytic gradient for this scheme, and apply it to geometry optimization of a silicon nanowire. In addition, we study the effect of the fragmentation to provide the guidelines for future applications of FMO/AFO.

2. Methodology

2.1. Theory and implementation

In the two-body FMO expansion, FMO2, denoted by FMO2-RHF if restricted Hartree–Fock (RHF) is used, the energy of N fragments is given by [14]:

$$E = \sum_I^N E_I + \sum_{I>J}^N (E_{IJ} - E_I - E_J) \tag{1}$$

where E_I and E_{IJ} are the monomer (single fragment) and dimer (fragment pair) energies, respectively, computed in the electrostatic field of other fragments. The energy gradient of Eq. (1) is computed in a straightforward fashion with a small approximation regarding the coupling of the electrostatic potentials and the fragment densities [28,34,35], with the appropriate frozen orbital treatment [36]. The expansion in Eq. (1) can be extended to include trimer corrections [18].

Practically, the calculations are performed as follows: from the atomic coordinates and the list of pairs of atoms between which covalent bonds are detached, small model systems containing each of such bonds are automatically constructed, and the detached bond orbitals are extracted from the localized orbitals of these model systems and consequently frozen in FMO calculations [33]. Fragment calculations are performed self-consistently until the fragment densities determining the electrostatic field converge, followed by calculations of fragment pairs. From these monomer and dimer calculations, the total energy E in Eq. (1) and the total

gradient ∇E are computed [35] and used in the standard optimization engines. FMO/AFO input files can be made using freely distributed FACIO modeling software [37].

The gradient of FMO/AFO was developed in GAMESS-US [38] and parallelized using the generalized distributed data interface [39]. Optimizations were performed until the maximum gradient element and RMS gradient dropped below 10^{-4} and $1/3 \times 10^{-4}$ a.u., respectively. For density functional theory (DFT) we used the B3LYP functional and the SG-1 grid, as implemented in GAMESS [38]. B3LYP is thought to give reasonable structures, which is the main goal of this study. All calculations were done on the Soroban cluster (AIST) consisting of 13 dual quad-core 2.66 GHz Xeon nodes with 16 GB RAM per node, connected by dual Gigabit Ethernet.

2.2. Error analysis

To analyze the accuracy, we define the errors in the total energy, E, dipole moment, d, and gradient, G, and the interfragment charge transfer, Q,

$$\Delta E = E^{\text{FMO2-RHF}} - E^{\text{RHF}} \tag{2}$$

$$\Delta d_n^{\text{RMS}} = \sqrt{\frac{|\mathbf{d}^{\text{FMO}n\text{-RHF}} - \mathbf{d}^{\text{RHF}}|^2}{3}} \tag{3}$$

$$\Delta \bar{Q} = \sum_I^N |\sum_{I \neq J}^N \Delta Q_{IJ}| \tag{4}$$

$$\Delta Q = \sum_{I>J}^N |\Delta Q_{IJ}| \tag{5}$$

$$\Delta G^{\text{RMS}} = \sqrt{\frac{|\nabla E^{\text{FMO2-RHF}} - \nabla E^{\text{RHF}}|^2}{3N_{\text{AT}}}} \tag{6}$$

$$\Delta G^{\text{MAX}} = \max(|\nabla_i E^{\text{FMO2-RHF}} - \nabla_i E^{\text{RHF}}|) \tag{7}$$

where the many-body expansion level n is 1 or 2 (dipole moments are also obtained analogously to Eq. (1), with the FMO1 values ($n = 1$) corresponding just to the monomer sum and $n = 2$ giving FMO2 dipoles. ΔQ_{IJ} is the charge transfer value from fragment I to fragment J. N_{AT} is the number of atoms, i runs through $3N_{\text{AT}}$ atomic coordinates. Since $\mathbf{d}^{\text{RHF}}$ is zero for this system without fragmentation, Δd_n^{RMS} coincides with the RMS of the FMO-RHF dipole moment. DFT quantities can be defined in the same way.

Typically, the two ΔQ quantities have similar values (usually, $\Delta \bar{Q} \leqslant \Delta Q$), except for some interesting cases with symmetry, such as the cyclic charge transfer [17]. As the FMO expansion is based on determining the electrostatic environment for fragments, whose total electron count is fixed, the charge transfer in pair calculations (ΔQ_{IJ}) gives a measure of the accuracy of the fragmentation; ideally, $\Delta Q_{IJ} = \Delta \bar{Q} = \Delta Q = 0$. Finally, we note that ΔQ and $\Delta \bar{Q}$ values are of particular interest because they are computed only from the FMO results, giving some measure of the error without calculating the same system with ab initio.

3. Application to silicon nanowires

3.1. Introductory remarks

Low-dimensional nanoscale objects like semiconductor quantum dots and nanowires with effective dimensions of 1–100 nm constitute a new fast-growing research area in condensed-matter physics and material science [40,41]. Modern semiconductor pro-

cessing techniques enable the electron quantum confinement. In particular, such finite fermion systems have much in common with atoms, yet they are man-made structures, designed and fabricated in the laboratory.

The electronic structure of silicon nanowires have been studied using a wide variety of models (empirical potentials, k–p and tight binding (TB) models, semiempirical methods, DFT, and the GW method, see [42]). For the cluster models ($\sim 10^3$ atoms) with the effective sizes close to real systems (1–8 nm) mostly model potential or empirical models like TB have been used, and recent progress has extended the applicability of ab initio methods to nanoscale objects of real sizes (2–3 nm and larger).

Typically, simple structural models, cut out from silicon crystalline lattice along the $\langle 1\,1\,1 \rangle$, $\langle 1\,1\,0 \rangle$ and $\langle 1\,0\,0 \rangle$ directions, have been used for electronic structure calculations. Because of the well-known fact that dangling bonds typically introduce surface states in the band gap, surface passivation with hydrogen is often applied to the nanowires in simulations, and surface effects determine many important characteristics of the electronic structure.

The nanowire piece used in this work and its fragmentation are shown in Fig. 1. Its chemical formula is $Si_{224}H_{162}$, and we divided it into 6 fragments of similar size (two of 73 and four of 60 atoms) and 12 fragments (two of 43 and ten of 30 atoms). The larger fragments (73 and 43 atoms, respectively) are terminal. In the following discussion we mainly use the 6-fragment division except where otherwise indicated. The optimizations were performed in C_1 symmetry and the optimized structures were found to be of nearly perfect C_{2h} symmetry. The number of spherical basis functions for the STO-3G and 3-21G* basis sets was 2178 and 4625, respectively.

3.2. Fragmentation and accuracy

There are two main factors controlling the AFO scheme in FMO [33]: (a) the size of the model system and (b) the extent of expanding (spanning) the frozen orbitals over AOs. In addition, there is freedom in choosing the bond detachment positions. In this work, we divided the nanowire along its length into slices. There is a difference in detaching an A–B bond either at atom A or at B. To guide future applications, we performed a number of test calculations varying the fragmentation parameters and evaluated the accuracy. The results are summarized in Table 1.

It is not sufficient to look at just the energy, as due to a fortuitous error cancellation the error can be misleadingly small. The dipole moment gives a reasonable indication of the accuracy of the density distribution, and the charge transfer quantifies the appropriateness of the fragmentation. The gradient errors obviously are linked to the quality of the optimized structures, and because the maximum gradient errors were (for 6 fragments, see Table 1) about 10^{-3} a.u/bohr among all atoms (including those which form detached bonds), with a root-mean-square deviation (RMSD) of 2×10^{-4} a.u/bohr, the optimized structures can be expected to be nearly equal to those obtained with ab initio methods.

The model system, which is automatically constructed by the program around each detached bond (e.g., see Fig. 2a), can be small (Fig. 2b) or large (Fig. 2d). Also, it can be large from the side of either the bond-detached atom (BDA) or bond-attached atom (BAA), and small from the other (Fig. 2c). In FMO, covalent bonds are detached heterolytically, by placing the two electrons (assuming single bonds) to the fragment to which BAA is assigned. For the silicon nanowire, two types of cross-sections were tried (Fig. 3): zigzag, where the choice of cutting A–B bonds across the nanowire either at A or at B was alternated between the two fragments, and unilateral, where all bonds were cut so that the left fragment had all BDAs and the right all BAAs.
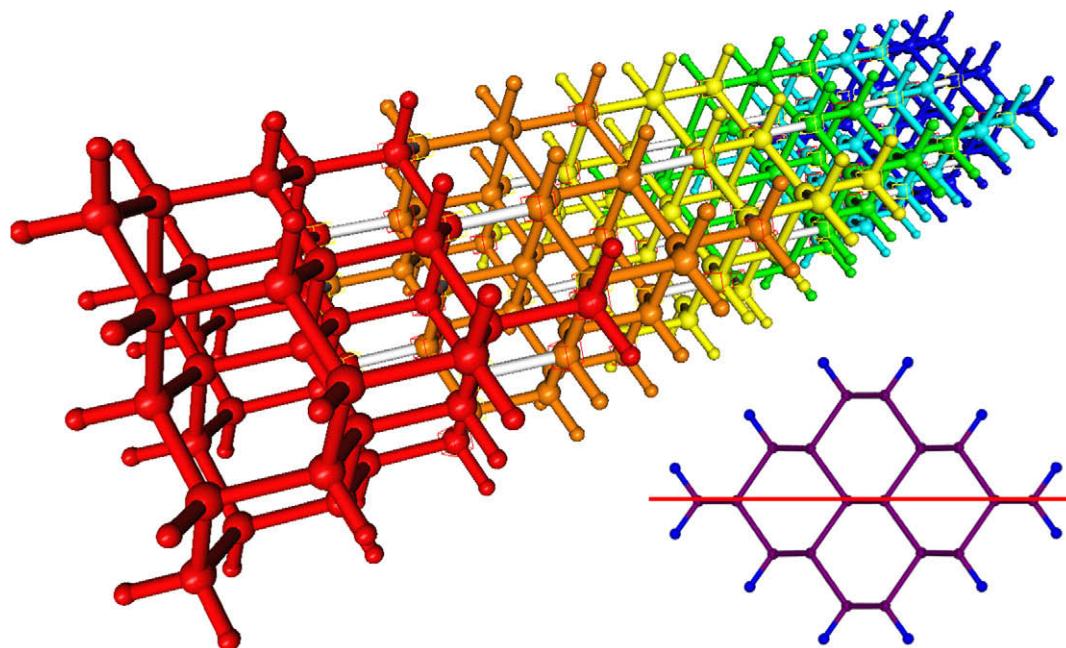
Fig. 1. Silicon nanowire fragmented for FMO calculations, where fragments are marked in different colors. Detached bonds are in gray and the lower part gives a facet view with the plane of symmetry shown as a red line (C_{2h} point group). (For interpretation of the references to color in this figure legend, the reader is referred to the web version of this article.)

Table 1
Dependence of the errors[a] upon the fragmentation in FMO2-RHF/AFO, defined by the model, section (nanowire cutting edge), AO span of frozen orbitals describing detached bonds and the number of fragments.

Model	Large	Large	Large-BDA	Large-BAA	Small	Small	Small	Small	Small	Small
Section	Zigzag[b]	Zigzag[b]	Zigzag[b]	Zigzag[b]	Zigzag[b]	Zigzag[b]	unilateral[c]	Zigzag[d]	Zigzag[e]	Zigzag[f]
AO span	Wide	Narrow	Wide	Wide	Wide	Narrow	Narrow	Narrow	Narrow	Narrow
Basis set	3-21G*	3-21G*	3-21G*	3-21G*	3-21G*	3-21G*	3-21G*	STO-3G	STO-3G	STO-3G
Fragments	6	6	6	6	6	6	6	12	12	12
ΔE	−1.9	−2.0	−0.8	−2.7	−2.4	−2.3	−4.1	340.1(−2.8)[g]	459.0	319.6
Δd_1^{RMS}	1.5	1.9	0.8	1.1	1.2	1.8	10.7	5.6	5.6	62.4
Δd_2^{RMS}	0.3	0.3	0.1	0.1	0.2	0.3	4.9	2.1(0.8)[g]	2.1	19.7
$\Delta \bar{Q}$	0.34	0.14	0.63	0.44	0.36	0.20	0.35	0.31	1.12	0.29
ΔQ	0.29	0.09	0.49	0.50	0.35	0.15	0.41	0.33	0.72	0.51
ΔG^{MAX}	1.22	0.79	1.40	0.88	0.89	0.89	4.38	7.38	7.97	7.68
ΔG^{RMS}	0.16	0.16	0.17	0.16	0.16	0.17	0.51	2.17	2.08	2.25

[a] In energy ΔE (kcal/mol), dipole moment Δd_n^{RMS} (Debye), charges $\Delta \bar{Q}$ and ΔQ (a.u.) and gradient ΔG^{MAX} and ΔG^{RMS} (10^{-3} a.u./bohr).
[b] Fig. 3d.
[c] Fig. 3b.
[d] Fig. 3e.
[e] Fig. 3f.
[f] As in Fig. 3e, but BDAs and BAAs are switched around for the 5 rightmost sections.
[g] With three-body corrections (FMO3).

In addition, in the zigzag scheme we followed the system symmetry (C_{2h}) as much as possible, by defining bond detachment symmetrically with respect to all point group operations, with the exception of the central section (between fragments 3 and 4). As the bond detachment in FMO is heterolytic and asymmetric, it was not possible to preserve the symmetry for this central section. Fragments 1 and 6, or 2 and 5 are thus completely symmetric; fragments 3 and 4 differ a little in the bond detachment details (see Fig. 3, fragments are numbered from right to left). Typical fragments are shown in Fig. 4.

Finally, two orbital spanning schemes were tested: wide, in which all atoms in the model system were used to expand the frozen orbitals (except those capping atoms, which are hydrogen in the model systems but silicon in the full system), and narrow, in which only BDA and BAA AO coefficients were used (Fig. 5).

As for the comparison of the zigzag and unilateral sections, we see in Table 1 that the former had consistently smaller errors when comparing the two sections for the small model/ narrow span, thus we used the zigzag section in the following tests. The reasons for the better performance of the zigzag scheme are twofold: further separation of the detached bonds (see Fig. 3, BDAs are close in the unilateral and alternated in the zigzag schemes, along each section) and the conservation of symmetry. The former is thought to be the major factor; the latter plays some role too, especially for the division into 12 fragments (apparently not very important for 6). The unilateral asymmetric division creates a large dipole moment of 10.7 Debye (Table 1) at the one-body level (i.e., the sum of fragment dipoles), which is only partially recuperated by the two-body corrections (to 4.9 Debye). All zigzag schemes had small total dipole moments (the *ab initio* dipole moment of this system is zero). Although the total dipole moment of the nanowire was small, which means that the overall electrostatic environment was reasonable, the dipole on the two terminal fragments was large and opposite in direction, due to the presence of detached bonds on one side only.
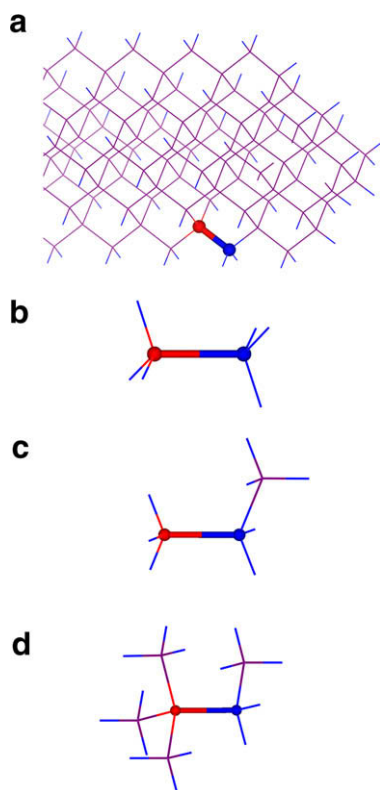
Fig. 2. Model system choice. (a) A close-up showing one bond to be detached, (b) the small model, (c) the large-BAA model and (d) the large model. BDA and BAA are shown in red and blue, respectively. (For interpretation of the references to color in this figure legend, the reader is referred to the web version of this article.)

Fig. 4. Typical fragment (except the two termini) for divisions into (a) 6 (see Fig. 3d) and (b) 12 (see Fig. 3e) fragments. Si and H atoms are shown in violet and blue, respectively. (For interpretation of the references to color in this figure legend, the reader is referred to the web version of this article.)

In the application of FMO/AFO to zeolites [33], the large model for detached bonds was used with the wide span. The advantage of larger models i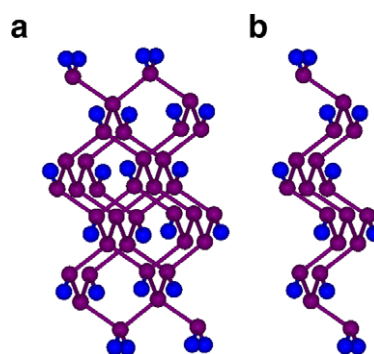s in a better inclusion of the effects of the environ-ment upon a given bond; thus it is especially advantageous to use them for very polar systems.

In this system the narrow span of the frozen localized orbitals had a slightly higher accuracy than the wide span, for both large and small models. The reason for this can be seen in Fig. 5c. For this system, the wide span results in the overlap of two model systems, not only in terms of atoms, which by itself causes no problem, but also in the AO span of the frozen orbitals; namely, the same atoms (e.g., BAA2 and BAA3) are used to span frozen orbitals for several model systems (i.e., several detached bonds). If the span is reduced from wide to narrow (Fig. 5b vs. a), the overlap of atoms disappears.

The most accurate fragmentation for this system was obtained by using the large model with the narrow span. The small model (chosen for geometry optimizations) with the narrow span was only slightly less accurate and had a very small cost to generate frozen orbitals. Enlarging the model system from either BDA or BAA side (large BDA and large-BAA, respectively) decreased some error criteria but increased others; we did not choose to employ these two models any further.
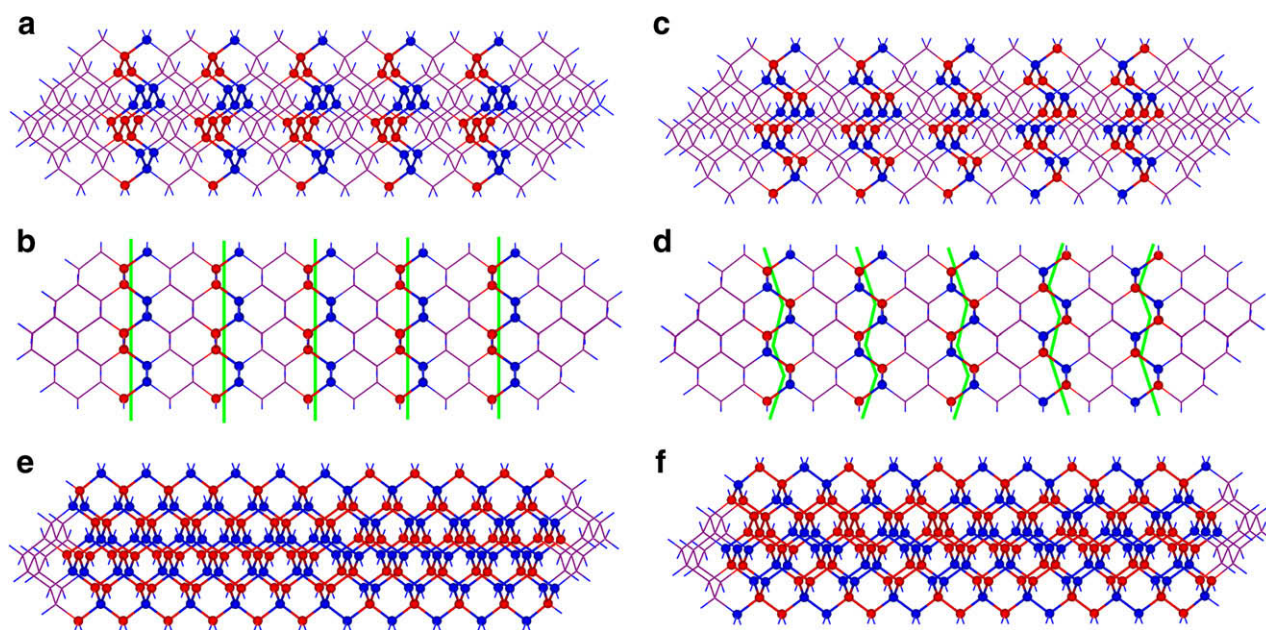

Fig. 3. Cross sections: (a) and (b) unilateral, (c) and (d) zigzag (all for division into 6 fragments). BDAs and BAAs are shown as red and blue spheres, respectively. Bonds are detached heterolytically at BDAs. The plane of parts (b) and (d) coincides with the plane of symmetry (C_{2h}). Cross sections for 12 fragments are shown in (e) and (f); both are zigzag and symmetric. (For interpretation of the references to color in this figure legend, the reader is referred to the web version of this article.)
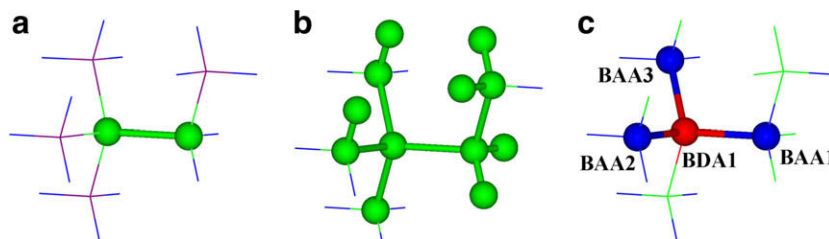
Fig. 5. Extent of the AO span of frozen orbitals for the large model. Atoms are shown in green, for which AOs are used to expand (span) frozen orbitals, in (a) narrow span and (b) wide span. (c) BAAs from other fragmented bonds (BAA2 and BAA3) are used to span frozen orbitals for the detached bond determined by BDA1 and BAA1 for the wide span. (For interpretation of the references to color in this figure legend, the reader is referred to the web version of this article.)

3.3. Many-body corrections

Next, we discuss the many-body corrections. Because of the linear shape of the system, for the 6-fragment division the number of SCF dimers is $N − 1$ ($I, I + 1$ dimers, other pairs are treated with the electrostatic approximation [17]), which gives ~10–17 kcal/mol repulsion between $I, I + 2$ pairs (RHF/STO-3G). For 12 fragments, the latter type of dimers ($I, I + 2$) is treated by SCF, so that the total number of SCF dimers is $2N − 3$. The number of trimers is N-2, because we set the trimer threshold in such a way to compute only connected [16] fragments, i.e. $I, I + 1, I + 2$ (other trimers contribute little). The large repulsion between $I, I + 2$ dimers (34–46 kcal/mol) is likely to be the reason for the large error in the energy for the division into 12 fragments; it is properly reduced by the negative trimer corrections (33–49 kcal/mol each).

In terms of the computational costs, FMO3 calculation is not expensive due to the small number of trimers: FMO2 and FMO3 took 47 and 72 min, respectively (single point RHF/STO-3G, 12 fragments, on 3 dual quad-core 2.66 GHz Xeon nodes). FMO2 with 6 fragments took 105 min, and *ab initio* calculation took 117 min. Nearly linear scaling of FMO [17] would make its efficiency much more prominent for larger systems.

3.4. Results of structure optimization

We used the optimum fragmentation scheme (large model, narrow span, zigzag section) for the full geometry optimizations using FMO/AFO with STO-3G and 3-21G* for both RHF and DFT. The obtained results are compared to other available data in Table 2. The purpose of using a small basis set (STO-3G) is to see if it can be used for preliminary studies, such as the initial structure preparation for the optimization with larger basis sets.

At the RHF level, when comparing STO-3G with 3-21G*, one can see that in the latter case the Si–Si bonds are shorter by ~0.010 Å

and the Si–H bonds are longer by ~0.011 Å. RMSD between the 3-21G* and STO-3G structures is 0.0922 Å, which indicates that they are similar. Both possess C_{2h} symmetry with an averaged deviation of ~0.005 Å. The Si–Si bond length obtained with 3-21G* (2.355 Å) is in reasonable agreement with the experimental measurement of 2.347 Å, and is also comparable to other calculations.

We note the effect of the surface tension upon the observed variation in the bond lengths. The surface reconstruction of silicon crystal has been studied extensively by theory and experiment [43–45]. Using the STM experimental technique, the Si(1 1 1) (1 × 1) and Si(0 0 1) (1 × 1) surface reconstructions of the thin ⟨1 1 0⟩ oriented Si nanowires were qualitatively analyzed in [46].

At the RHF/3-21G* level, the Si–H bond lengths for 26 –SiH$_2$ groups vary within 1.482–1.484 Å, whereas those for 110 –SiH groups were 1.486–1.488 Å. Thus, we see that the values are directly affected by the number of passivating hydrogens per silicon atom; having two H atoms vs. one shortens the bond length by ~0.004 Å.

The observed difference in the Si–Si bond lengths is much more pronounced. For Si atoms in –SiH$_2$ groups, Si–Si bond lengths (representing the surface to bulk bonding, where we refer to hydrogenated silicon atoms as *surface* and to other Si atoms as *bulk*) varied within 2.348–2.355 Å. For Si atoms in –SiH groups, they were 2.350–2.358 Å, which is marginally longer than for –SiH$_2$ groups. However, for bulk Si (88 atoms) the Si–Si bond lengths (bulk to bulk, excluding those involving surface Si) were somewhat longer, 2.355–2.363 Å. The longest Si–Si bond length (2.363 Å) was found exactly in the middle of the nanowire (bulk Si); it is the closest representative of bulk crystalline silicon in our nanowire. We did not discern any systematic difference in the geometric parameters when comparing the two facets with other surfaces of the nanowire.

Thus, we conclude that the passivation by hydrogen has the following effects upon geometry. In comparison with the bulk silicon

Table 2
Comparison of the bond lengths R in silicon systems (averaged values are in parentheses).

System	Thickness × length (nm)	Method	Reference	R(Si–Si) (Å)	R(Si–H) (Å)
⟨1 1 0⟩ nanowire	1.2 × 4.8	FMO-RHF/STO-3G 6 fragments[a]	This work	2.358–2.376 (2.365)	1.473–1.476 (1.474)
⟨1 1 0⟩ nanowire	1.2 × 4.8	FMO-RHF/3-21G* 6 fragments[a]	This work	2.348–2.363 (2.355)	1.482–1.488 (1.485)
⟨1 1 0⟩ nanowire	1.2 × 4.8	FMO-B3LYP/STO-3G 6 fragments[a]	This work	2.354–2.378 (2.364)	1.492–1.497 (1.495)
⟨110 ⟩ nanowire	1.2 × 4.8	FMO-B3LYP/3-21G* 6 fragments[a]	This work	2.323–2.350 (2.339)	1.492–1.500 (1.496)
⟨1 1 0⟩ nanowire	1.2 × 4.8	FMO-B3LYP/STO-3G 12 fragments[a]	This work	2.351–2.411 (2.368)	1.492–1.498 (1.496)
⟨1 1 0⟩ nanowire	1.2 × 1D periodic (c = 0.3847)[b]	LDA PP PAW	[47]	2.33–2.34	1.51
⟨1 1 0⟩ nanowire	1.2 × (0.8–2.0)	B3LYP/3-21G*	[46]	2.310–2.500	1.496
⟨1 1 0⟩ nanowire	(1.3–7.0) × 1D periodic	STM experimental estimate[c]	[48]	2.347	–
3D crystal	c = 0.5430[b]	LDA PP PAW	[46]	2.35	–
3D crystal	c = 0.5430[b]	LDA PAW	[49]	2.35	–
3D crystal	c = 0.543095[b]	Experiment	[50]	2.352	–

[a] Small model, narrow span, zigzag section.
[b] Lattice constant (nm).
[c] Passivated by –CH$_3$, Si(1 1 1) (1 × 1) and Si(0 0 1) (1 × 1) surface reconstruction, see [48].

atoms buried inside the nanowire, the Si–Si bonds for directly hydrogenated Si atoms are shortened by ∼0.01 Å (∼0.008 Å in average for all Si atoms). This agrees with the experiment (crystal: 2.352 Å, nanowire (averaged over all atoms) 2.347 Å, the difference being 0.005 Å). The observed difference from the experiment (0.008 vs. 0.005 Å) may be ascribed to the larger experimental thickness of nanowires, which decreases the fraction of the surface silicon atoms, and to the different passivation (by –CH_3). The shortening of the bond length can be interpreted as the stabilization of the Si–Si bonds upon hydrogenation, and it is slightly more pronounced for the Si atoms to which two hydrogens are attached.

As for the effect of the electron correlation treated with DFT/B3LYP and STO-3G, the error in the energy for the small model with the narrow span, zigzag section was 0.6 kcal/mol (compared to B3LYP without fragmentation). As listed in Table 2, DFT compared with RHF elongates the Si–H bonds by 0.021 Å on the average, and only insignificantly shortens the Si–Si bonds (by 0.001 Å). RMSD of the RHF and DFT structures was 0.0307 Å, clearly caused by the difference in the Si–H bond lengths, and a good agreement with the B3LYP/3-21G* results [46] is observed. At the 3-21G* level, the RMSD between FMO-RHF and FMO-B3LYP was 0.112 Å, nearly equally caused by the changes (RHF → DFT) in the Si–H and Si–Si bond lengths, which were elongated by 0.011 Å and shortened by 0.015 Å, respectively.

To summarize, the Si–Si bonds were nearly evenly affected by both the basis set and the method (RHF vs. DFT), whereas the Si–H bonds were affected mainly by the method but insignificantly by the basis set change. A short length of nanowires 0.8–2.0 nm [46] vs. 4.8 nm in this work promotes too strong surface effects (i.e., elongated Si–Si bonds, up to 2.500 Å) to be representative of realistic nanowires. Our geometries agree reasonably with LDA PP PAW [47], where the periodic system was considered.

We also exploited the possibility of reducing the fragment size further by dividing the nanowire into 12 fragments, which greatly speeds up the calculations. As listed in Tables 1 and 2, the energy is not well reproduced, but the gradient has fairly small errors. The asymmetric zigzag sections (the last column in Table 1) produced a very significant error in the dipole moment, and the best fragmentation was found to be that shown in Fig. 3e, where the symmetric zigzag section had detached bonds separated as far as possible (using the small model and narrow span).

RMSD for the optimized DFT/STO-3G structures with 6 and 12 fragments was 0.0767 Å. The Si–H bond lengths are affected very slightly by the increased number of fragments, whereas the Si–Si bonds show a considerable difference. A majority of the Si–Si bonds are reasonable, as also observed in that the average for 12 fragments is close to that of 6 fragments, but a portion of them is elongated, due to the repulsion between the fragments that adds stress upon the structure, as revealed in the large energy errors.

We note that the bonds with large errors are different from bonds which are detached. The detached bond lengths are well corrected by dimer calculations and have values on the order of 2.36–2.37 Å. The worst cases are found for the Si–Si bonds on BAAs and BDAs (i.e., other than the detached bonds), because they are recovered insufficiently by the dimer calculations. We thus conclude that the divisions into small fragments may be useful for modeling, but it is advisable to use large enough fragments for a further structure refinement.

4. Conclusions

We have developed and implemented analytic gradients for the FMO/AFO method that are applicable to covalent crystals, surfaces and related systems. To guide future applications, we have performed a number of tests for various fragmentation schemes, high-lighted the reasons for the observed differences in the accuracy, and determined the optimum scheme, for which the errors vs. *ab initio* values without fragmentation are found to be very small.

As an application, we have optimized the structure of a small silicon nanowire and examined the basis set and electron correlation effects. We find that even a small basis set such as STO-3G works quite well in this system, in comparison with a larger basis set (3-21G*) and experiment. The geometrical parameters have been analyzed in detail, and the effects of hydrogen passivation upon the structure are discussed and compared with experiment and other calculations. One of the findings is that hydrogenation of nanowires leads to the shortening of the Si–Si bond lengths and stabilizing them in comparison with the bulk silicon, and that the effect is more pronounced for those atoms where two hydrogen atoms are attached. It should also be noted that there is an indication that pure silicon nanowires (without hydrogen) are also stabilized vs. bulk silicon due to the reconstruction of the surface.

While silicon nanowires alone are perhaps not a very sophisticated object, the computational scheme developed in the present study can be applied to more complex nanosystems interfacing nanowires with other systems. An important property is the band gap, which can be studied by FMO in the many-body fashion, by considering the band gap in monomers and dimers (the latter giving some measure of many-body effects), or by computing molecular orbitals for a part or the whole system [25].

References

[1] E. Nikitina, V. Sulimov, V. Zayets, N. Zaitseva, Int. J. Quant. Chem. 97 (2004) 747.
[2] T. Nakajima, K. Hirao, Chem. Phys. Lett. 427 (2006) 225.
[3] T. Inaba, F. Sato, J. Comput. Chem. 28 (2007) 984.
[4] J. Jiang, K. Liu, W. Lu, Y. Luo, J. Chem. Phys. 124 (2006) 214711.
[5] V. Pomogaev, A. Pomogaeva, Y. Aoki, J. Phys. Chem. A 113 (2009) 1429.
[6] M. Kamiya, S. Hirata, M. Valiev, J. Chem. Phys. 128 (2008) 074103.
[7] E.E. Dahlke, H.R. Leverentz, D.G. Truhlar, J. Chem. Theor. Comput. 4 (2008) 33.
[8] L. Huang, L. Massa, J. Karle, Proc. Natl. Acad. Sci. USA 105 (2008) 1849.
[9] C.R. Jacob, L. Visscher, J. Chem. Phys. 128 (2008) 155102.
[10] W. Hua, T. Fang, W. Li, J.-G. Yu, S. Li, J. Phys. Chem. A 112 (2008) 10864.
[11] A.P. Rahalkar, V. Ganesh, S.R. Gadre, J. Chem. Phys. 129 (2008) 234101.
[12] P. Söderhjelm, U. Ryde, J. Phys. Chem. A 113 (2009) 617.
[13] M.S. Gordon, J. M. Mullin, S.R. Pruitt, L.B. Roskop, L.V. Slipchenko, J.A. Boatz, J. Phys. Chem. B, in press, doi:10.1021/jp811519x.
[14] K. Kitaura, E. Ikeo, T. Asada, T. Nakano, M. Uebayasi, Chem. Phys. Lett. 313 (1999) 701.
[15] D.G. Fedorov, K. Kitaura, J. Phys. Chem. A 111 (2007) 6904.
[16] D.G. Fedorov, K. Kitaura, in: E.B. Starikov, J.P. Lewis, S. Tanaka (Eds.), Modern Methods for Theoretical Physical Chemistry and Biopolymers, Elsevier, Amsterdam, 2006, p. 3.
[17] D.G. Fedorov, K. Kitaura (Eds.), The Fragment Molecular Orbital Method: Practical Applications to Large Molecular Systems, CRC Press, Boca Raton, FL, 2009.
[18] D.G. Fedorov, K. Kitaura, J. Chem. Phys. 120 (2004) 6832.
[19] D.G. Fedorov, K. Kitaura, Chem. Phys. Lett. 389 (2004) 129.
[20] D.G. Fedorov, K. Kitaura, J. Chem. Phys. 121 (2004) 2483.
[21] D.G. Fedorov, K. Kitaura, J. Chem. Phys. 122 (2005) 054108.
[22] Y. Mochizuki, S. Koikegami, S. Amari, K. Segawa, K. Kitaura, T. Nakano, Chem. Phys. Lett. 406 (2005) 283.
[23] D.G. Fedorov, K. Kitaura, J. Chem. Phys. 123 (2005) 134103.
[24] M. Chiba, D.G. Fedorov, T. Nagata, K. Kitaura, Chem. Phys. Lett. 474 (2009) 227.
[25] S. Tsuneyuki, T. Kobori, K. Akagi, K. Sodeyama, H. Terakura, H. Fukuyama, Chem. Phys. Lett. 476 (2009) 104.
[26] Y. Mochizuki, K. Fukuzawa, A. Kato, S. Tanaka, K. Kitaura, T. Nakano, Chem. Phys. Lett. 410 (2005) 247.

[27] D.G. Fedorov, K. Kitaura, J. Comput. Chem. 28 (2007) 222.
[28] D.G. Fedorov, T. Ishida, M. Uebayasi, K. Kitaura, J. Phys. Chem. A 111 (2007) 2722.
[29] Y. Komeiji, Y. Mochizuki, T. Nakano, D.G. Fedorov, J. Mol. Struct. (THEOCHEM) 898 (2009) 2.
[30] N. Taguchi et al., J. Phys. Chem. B 113 (2009) 1153.
[31] A. Tagami et al., Chem. Phys. Lett. 472 (2009) 118.
[32] X. He, L. Fusti-Molnar, G. Cui, K.M. Merz Jr., J. Phys. Chem. B 113 (2009) 5290.
[33] D.G. Fedorov, J.H. Jensen, R.C. Deka, K. Kitaura, J. Phys. Chem. A 112 (2008) 11808.
[34] K. Kitaura, S.-I. Sugiki, T. Nakano, Y. Komeiji, M. Uebayasi, Chem. Phys. Lett. 336 (2001) 163.
[35] T. Nagata, D.G. Fedorov, K. Kitaura, Chem. Phys. Lett. 475 (2009) 124.
[36] V. Kairys, J.H. Jensen, J. Phys. Chem. A 104 (2000) 6656.
[37] M. Suenaga, J. Comput. Chem. Jpn. 7 (2008) 33 (in Japanese), Facio 11.8.8: <http://www1.bbiq.jp/zzzfelis/Facio.html>.
[38] M.W. Schmidt et al., J. Comput. Chem. 14 (1993) 1347.
[39] D.G. Fedorov, R.M. Olson, K. Kitaura, M.S. Gordon, S. Koseki, J. Comput. Chem. 25 (2004) 872.
[40] B.K. Teo, Coord. Chem. Rev. 246 (2003) 229.
[41] W. Lu, C.M. Lieber, J. Phys. D: Appl. Phys. 39 (2006) R387.
[42] L.C.L.Y. Voon, Y. Zhang, B. Lassen, M. Willatzen, Q. Xiong, P.C. Eklund, J. Nanosci. Nanotechnol. 8 (2008) 1.
[43] D.J. Chadi, Phys. Rev. Lett. 43 (1979) 43.
[44] G. Binnig, H. Rohrer, Ch. Gerber, E. Weibel, Phys. Rev. Lett. 50 (1983) 120.
[45] K.D. Brommer, M. Needels, B. Larson, J.D. Joannopoulos, Phys. Rev. Lett. 68 (1992) 1355.
[46] P.B. Sorokin, P.V. Avramov, L.A. Chernozatonskii, D.G. Fedorov, S.G. Ovchinnikov, J. Phys. Chem. A 112 (2008) 9955.
[47] P.B. Sorokin, P.V. Avramov, A.G. Kvashnin, D.G. Kvashnin, S.G. Ovchinnikov, A.S. Fedorov, Phys. Rev. B 77 (2008) 235417-1.
[48] D.D.D. Ma, C.S. Lee, F.C.K. Au, S.Y. Tong, S.T. Lee, Science 299 (2003) 1874.
[49] T. Vo, A.J. Williamson, G. Galli, Phys. Rev. B 74 (2006) 045116.
[50] C.R. Hubbard, H.E. Swanson, F.A. Mauer, J. Appl. Crystallogr. 8 (1975) 45.